

## Supplementary Information

### **“Uncapped” metal-organic frameworks (MOFs) dispersions driven by O<sub>2</sub> plasma towards superior oxygen evolution electrocatalysis**

Shan Ding, Yuxiang Zhang, Fengqian Lou, Muhammad Kashif Aslam, Yuntong Sun,

Ming Li, Jingjing Duan,\* Yibing Li,\* and Sheng Chen\*

Key Laboratory for Soft Chemistry and Functional Materials (Ministry of Education), School of Chemistry and Chemical Engineering, School of Energy and Power Engineering, Nanjing University of Science and Technology, Nanjing, 210094, China

**E-mail:** [jingjing.duan@njust.edu.cn](mailto:jingjing.duan@njust.edu.cn) (J.D.); [yibing.li@swjtu.edu.cn](mailto:yibing.li@swjtu.edu.cn) (Y.L.);  
[sheng.chen@njust.edu.cn](mailto:sheng.chen@njust.edu.cn) (S.C.)

## I. Experimental Section

### 1. Theoretical predictions.

First-principles calculation was performed using Mede A-VASP based on DFT within the planewave basis set approach. Perdew-Burke-Ernzerhof (PBE) functional in combination with DFT + U approach were used for electron exchange-correlation within generalized gradient approximation (GGA) implemented in VASP package code. Specifically, the Conjugate Gradient update algorithm was used for the structural optimization of NiFe MOF. We used low precision for efficient computation and normal precision for accurate computation. The convergence is 0.05 for efficiency and accuracy computation and both efficiency and accuracy computation use 450 eV planewave cutoff. A Gaussian smearing with a width of 0.05 eV was also utilized. For the surface Brillouin zone integration, a  $1 \times 1 \times 1$  Monkhorst-Pack k-point mesh was used. The convergence criteria for electronic self-consistent iteration and ionic relaxation were set to  $10^{-5}$  eV. Hubbard-U correction method (DFT+U) was carried out to improve the description of highly correlated Ni/Fe 3d orbitals with the value of U set to 4.0/6.4 eV.

The atomic structure was visualized using the software Visualization for Electronic and Structural Analysis (VESTA). Figure 1a shows the theoretical models of pristine NiFe-MOF and NiFe-MOF with outer surface functionalization, obviously demonstrated that hydroxyl group instead of hydrogen atom on benzene ring.

The formation energy was calculated as

$$E_f = E_{\text{doped-MOF}} - E_{\text{MOF}} + mE_{\text{dopant}} - nE_{\text{substituted atom}}$$

Where  $E_f$  is the energy of formation,  $E_{\text{doped-MOF}}$  is the total energy of the -OH doped

on the MOF,  $E_{\text{MOF}}$  is the energy of undoped one,  $E_{\text{dopant}}$  and  $E_{\text{substituted atom}}$  are the energies of doped atoms and substituted atoms respectively. Therefore, the lowest formation energy is also found on carbon number 17.

Furthermore, the charge transfer in NiFe-MOF catalyst has been visualized by the charge density difference that is expressed as:

$$\Delta\rho = \rho(\text{NiFe-MOF}) - \rho(\text{Ni}) - \rho(\text{Fe}) - \rho(\text{O}) - \rho(\text{C}) - \rho(\text{H})$$

where  $\rho(\text{NiFe-MOF})$ ,  $\rho(\text{Ni}) - \rho(\text{Fe}) - \rho(\text{O}) - \rho(\text{S}) - \rho(\text{C}) - \rho(\text{H})$  are the undisturbed electron densities of NiFe-MOF, Ni, Fe, O, C, and H atoms, respectively.

## 2. Material Synthesis

**Synthesis of NiFe-MOF particles.** 1 mL of de-ionized (DI) water, 8mg of  $\text{Ni}(\text{Ac})_2 \cdot 4\text{H}_2\text{O}$  and 2 mg of  $\text{Fe}(\text{NO}_3)_3 \cdot 9\text{H}_2\text{O}$  were added into a vial (10 mL). Next, 10 mg of organic ligand (2,6-naphthalenedicarboxylate tetrahydrate) was added into the above mixed solution, and reacted at 60 °C for 20 h. After cooling down to room temperature, the products were collected and washed with copious DI-water.

**Plasma-driven tuning NiFe-MOF's oxygen percentages.** The NiFe-MOF particles were placed in a quartz cavity and bombarded by  $\text{O}_2$  plasma (100 W, gas flow rate of  $120 \text{ mL min}^{-1}$ ) for 0, 10, 15, 20, 25, 30 and 40 min, respectively. During this process, the oxygen radicals produced by  $\text{O}_2$  plasma, which can react with the ligand of MOFs, and generate hydroxyl group on the outer surface of MOFs. Next, the as-formed product was dispersed in water with the assistance of ultrasonication to form a colloidal suspension ( $\sim 0.084 \text{ mg mL}^{-1}$ ). The dispersible solution was dialyzed for 24 h to remove residual metal salts.

**Size fractionation of NiFe-MOF.** NiFe-MOF aqueous dispersion ( $\sim 0.084 \text{ mg mL}^{-1}$ , 10 mL) was mixed with diluted HCl (10  $\mu\text{L}$ , 0.001 M) overnight. During this process, part of large NiFe-MOF particles was precipitated. Both the sediment and the residual dispersion were collected and dialyzed with DI-water, which are defined as S-NiFe-MOF and L-NiFe-MOF.

**Extend the synthesis protocol to other MOFs.** An aqueous solution was made by 50 mg of  $\text{FeCl}_2 \cdot 4\text{H}_2\text{O}$  and  $\text{Ni}(\text{Ac})_2 \cdot 4\text{H}_2\text{O}$  in 20 mL of ethanol solution, in which 10 mL of ethanol solution containing 50 mg of 2,5-thiophene dicarboxylic acid ( $\text{C}_6\text{H}_4\text{O}_4\text{S}$ ) was added. The mixture was hydrothermally reacted at 150  $^\circ\text{C}$  for 12 h. After cool down to room temperature, the product was collected and washed by ethanol and water. The procedure for modified MOFs with oxygen species was similar to that of NiFe-MOF particles.

### 3. Physical Characterizations

Scanning electron microscopy was conducted on a field emission scanning electron microscope (FESEM, JEOL 7800F); transmission electron microscope (TEM) and high-resolution transmission electron microscope (HRTEM) were conducted on an aberration-corrected TEM (FEI Titan 80-300, 300 KV acceleration voltage); atomic force microscope was conducted on a Bruker D8 SPM; energy-dispersive X-ray spectroscopy (EDS) and element mapping were acquired on SEM (OXFORD X-Max<sup>N</sup> 150 10KV); X-ray diffractions were conducted on X-ray diffractometer (XRD, Smart lab 9 kw, 40 kV, 40 mA,  $\lambda=1.5418 \text{ \AA}$ ) with  $\text{Cu-K}\alpha$  radiation; X-ray photoelectron spectroscopy (XPS) was collected between 0 and 1400 eV on an Axis Ultra (Thermo ESCALAB 250XI) XPS spectrometer equipped with an Al  $\text{K}\alpha$  source (1486.6 eV); zeta potentials were monitored on a Malvern ZS 90 Zeta sizer Nano

series analyser; FT-IR spectra were recorded in a Thermofisher NICOLETIS 10 FTIR spectrometer.

#### 4. Electrochemical characterizations.

Electrochemical tests were performed on a CHI 760E electrochemical workstation. Specifically, the working electrode was prepared by solution casting method. Firstly, 5 mg of samples, 1 mg of acetylene black, 40  $\mu\text{L}$  of Nafion solution (5 wt%) were dispersed in 1 mL of isopropanol/DI-water (3:1 v/v) by ultrasonication for 30 min to form a uniform catalyst ink. Next, 40  $\mu\text{L}$  of the uniform catalyst ink was dropped to  $1 \times 1 \text{ cm}^2$  carbon paper with a loading of  $0.2 \text{ mg cm}^{-2}$ , which were dried under ambient condition overnight.

OER was studied in a standard three-electrode glass cell, which connected to a CHI 760 workstation using S- and L-NiFe-MOF as the working electrode, carbon rod as the counter electrode, Hg/HgO (1 M KOH) as the reference electrode, and 1M of KOH as the electrolyte.

The OER potentials *vs.*  $E_{\text{Hg/HgO}}$  measured in this study were converted to reversible hydrogen electrodes (RHE) according to  $\text{Potential} = E_{\text{Hg/HgO}} + 0.059 \text{ pH} + 0.098$ . Linear sweep voltammogram (LSV) plots and cyclic voltammogram (CV) were recorded at the scan rates of  $10 \text{ mV s}^{-1}$  from 1 to 1.8 V (*vs.* RHE). All LSV testing data were obtained with 85% *iR*-compensation.

Tafel plots are recorded with the linear portions at low overpotential fitted to Tafel equation ( $\eta = b \log j + a$ , where  $\eta$  is overpotential (V),  $j$  is current density ( $\text{mA cm}^{-2}$ ), and  $b$  is Tafel slope ( $\text{mV dec}^{-1}$ ). The long-term durability was evaluated by chronoamperometric response at 1.48 V (*vs.* RHE) for OER up to 100 hrs. The corresponding LSVs before and after electrochemical testing were conducted with

85%  $iR$ -compensation for comparison. Electrochemical impedance spectroscopy (EIS) was recorded under the following conditions: AC voltage amplitude 0 or 1.5 V, frequency ranges  $10^6$  to 1 Hz, and open circuit; the current densities were normalized to the geometrical area. In addition, the electric double layer capacitances ( $C_{dl}$ , mF  $\text{cm}^{-2}$ ) of working electrodes were obtained from double-layer charge-discharge diagram using CVs in a small potential range of 1.2~1.3 V (*vs.* RHE). The multi-potential steps of current densities at 10, 20, 50, 100 and 200 mA  $\text{cm}^{-2}$  were used to estimate the stability of catalysts.

## II. Supplementary Results

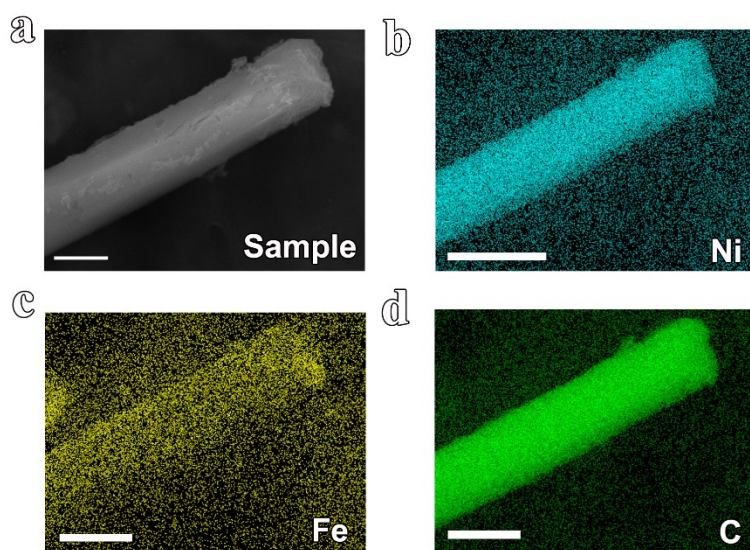


**Fig. S1.** Morphological characterization of NiFe-MOF treated by O<sub>2</sub> plasma for 20 min. a-d) SEM image and relevant element mapping of Ni, Fe and C taken from panel a) (scale bar: 1  $\mu\text{m}$ ).

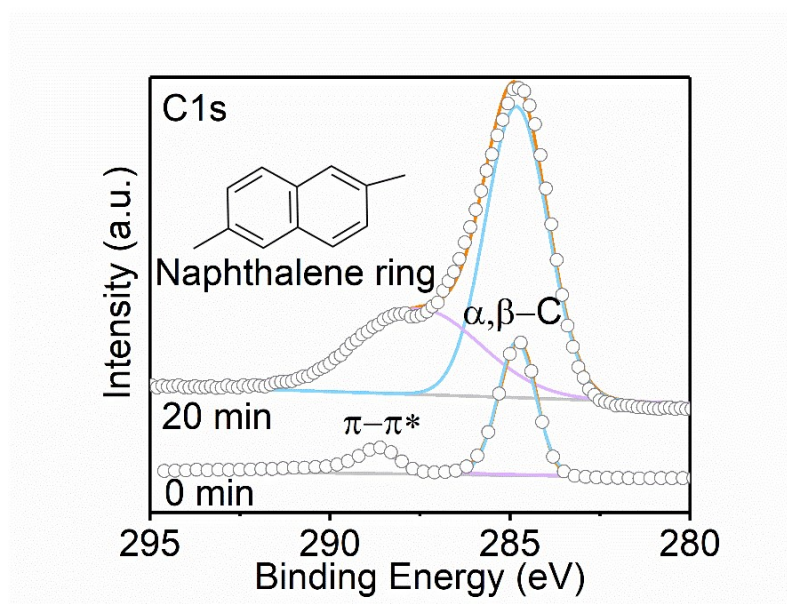


**Fig. S2.** The C1s spectra of NiFe-MOF treated by O<sub>2</sub> plasma for 0 and 20 mins, which exhibited the presence of  $\alpha, \beta$ -carbon and  $\pi$ - $\pi^*$  carbon originated from naphthalene ring of organic ligand.<sup>1</sup>

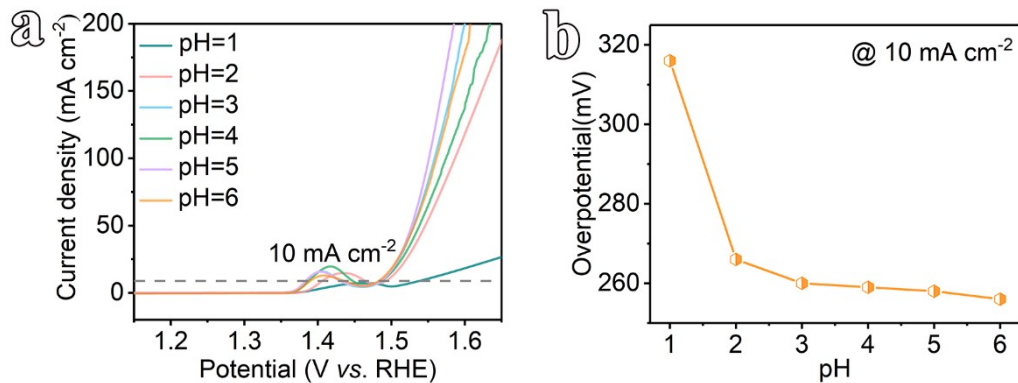


**Fig. S3.** The influence of OER performances on acid treatment for S-NiFe-MOF.

**Supplementary note:** To further study the influence of acid treatment, the as-obtained S-NiFe-MOF was dispersed into the diluted HCl solution (pH=1, 2, 3, 4, 5 and 6) overnight, and then the products were collected and washed by copious DI-water. The comparison of electrocatalytic performances between these samples for OER is presented by linear sweep voltammogram (LSV) plots (**Fig. S3**). Specifically, S-NiFe-MOF (pH=6) shows an overpotential of 256 mV at the current density of 10 mA cm<sup>-2</sup>, and S-NiFe-MOFs obtained at different pH ranging from 6 to 2 show similar performances (pH=5, 258 mV, pH=4, 259 mV, pH=3, 260 mV, pH=2, 266 mV @ 10 mA cm<sup>-2</sup>), and S-NiFe-MOF (pH=1) displayed a considerable overpotential of 316 mV @ 10 mA cm<sup>-2</sup>. Therefore, there is no negative effect of weak acid treatment (pH=6) during the process of size fractionation for S-NiFe-MOF.

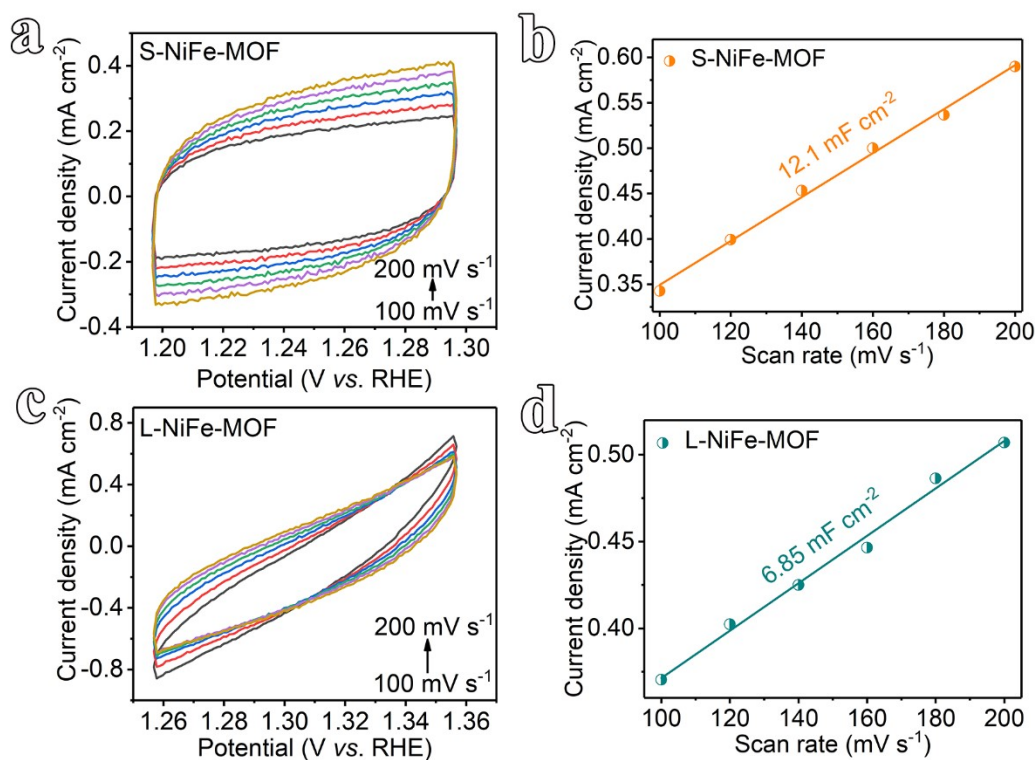


**Fig. S4.** Electric double layer capacitance of S- and L-NiFe-MOF in 1 M KOH electrolyte. a, b) S-NiFe-MOF; c, d) L-NiFe-MOF. Specifically, a, c) the corresponding CVs measured at different scan rates from 100 to 200  $\text{mV s}^{-1}$  at a potential range of 1.2~1.3 V, 1.26~1.36 V (vs. RHE); b, d) the current densities at 1.25 V, 1.31 V (vs. RHE) were plotted against scan rates.

**Supplementary note:** The  $C_{dl}$  value of the synthesized electrode was evaluated on the basis of CVs. The CVs of both samples display an analogous rectangular shape of an electrical double layer capacitor. In this potential region, charge transfer electrode reaction is considered to be negligible, and thus the current is solely from electrical double layer charging and discharging. The plot of current density against scan rate has a linear relationship, and the slope is the double layer capacitance. The values of

double layer capacitance are 12.1, 6.85 mF cm<sup>-2</sup> for S-NiFe-MOF and L-NiFe-MOF, respectively.

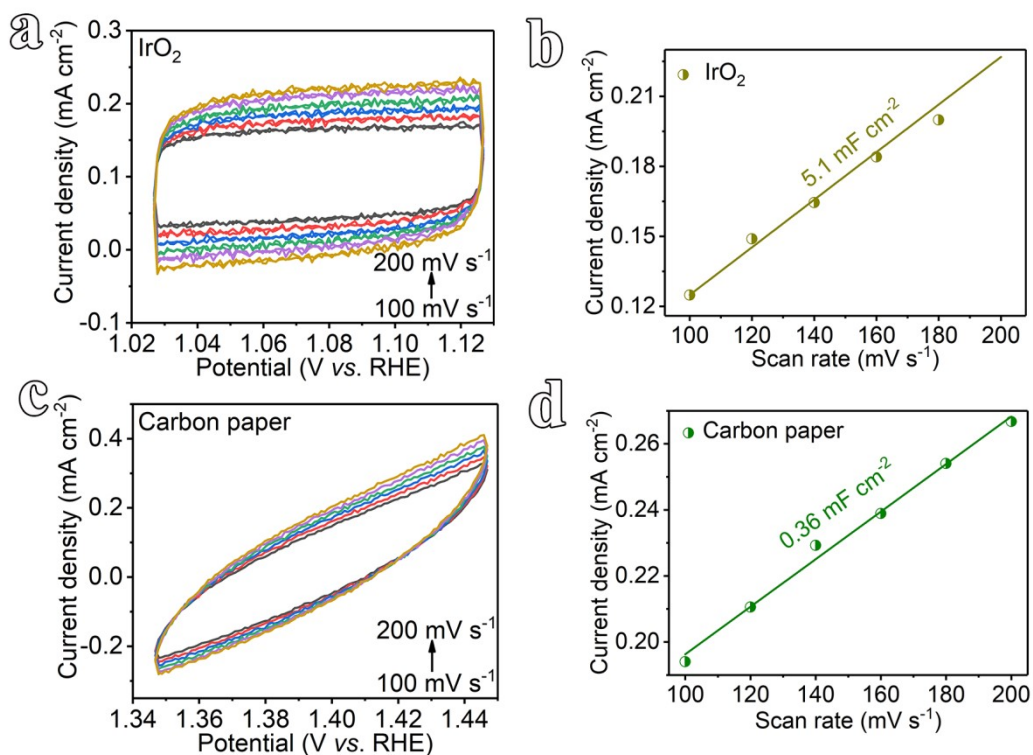


**Fig. S5.** Electric double layer capacitances of IrO<sub>2</sub> and carbon paper in 1 M KOH electrolyte. a, b) IrO<sub>2</sub>; c, d) Carbon paper. Specifically, a, c) the corresponding CVs measured at different scan rates from 100 to 200 mV s<sup>-1</sup> at a potential range of 1.03~1.13 V, 1.35~1.45 V (vs. RHE); b, d) the current densities at 1.08 V, 1.40 V (vs. RHE) were plotted against scan rates.

**Supplementary note:** The plot of current density against scan rate has a linear relationship, and the slope is the double layer capacitance. The values of double layer capacitance are 5.1, 0.36 mF cm<sup>-2</sup> for IrO<sub>2</sub> and Carbon paper, respectively.

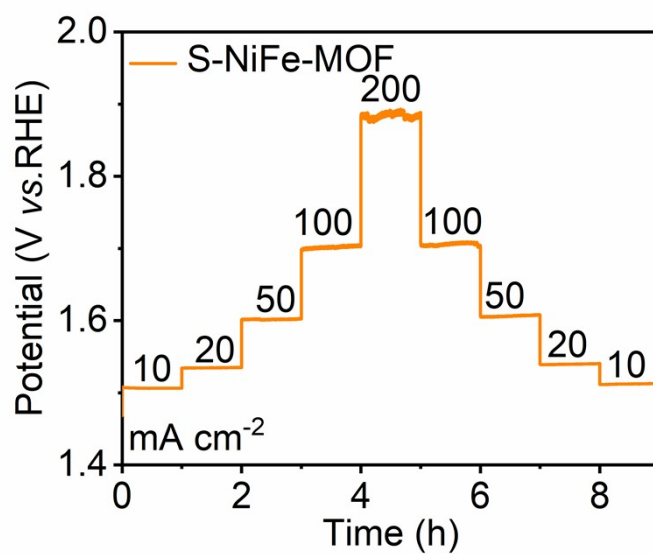


**Fig. S6.** The multi-potential steps of S-NiFe-MOF at the current densities of 10, 20, 50, 100 and 200 mA cm<sup>-2</sup>, respectively.

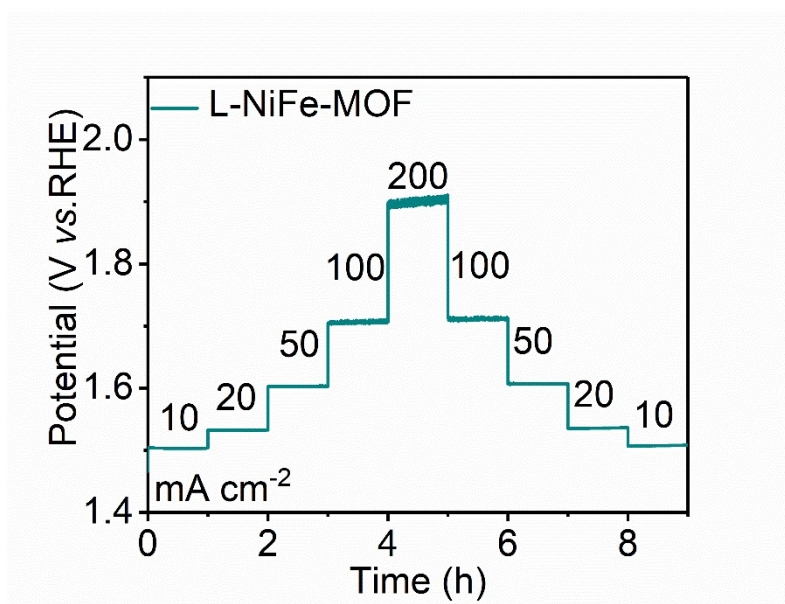


**Fig. S7.** The multi-potential steps of L-NiFe-MOF at the current densities of 10, 20, 50, 100 and 200 mA cm<sup>-2</sup>, respectively.

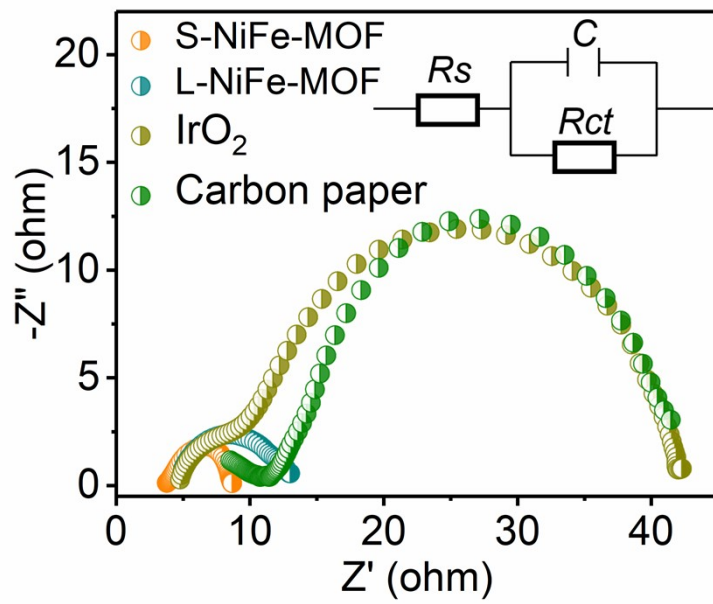


**Fig. S8.** Electrochemical impedance spectroscopy (EIS) spectra of different samples in 1 M KOH electrolyte under open circuit voltage, which indicates its faster electron transport and charge transfer during OER process.

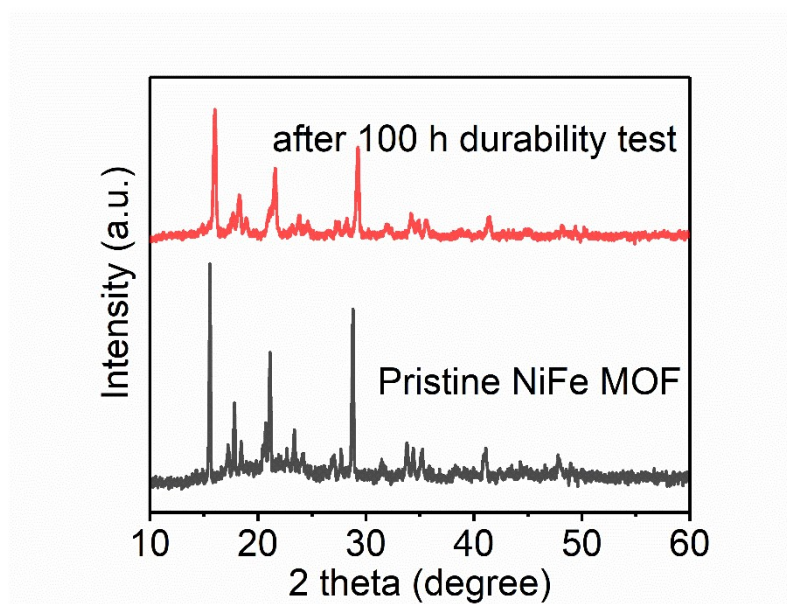


**Fig. S9.** XRD patterns of S-NiFe-MOF after 100 hrs durability test at current density of  $10 \text{ mA cm}^{-2}$  for OER in 1 M KOH electrolyte, which shows seldom structural change before and after test.

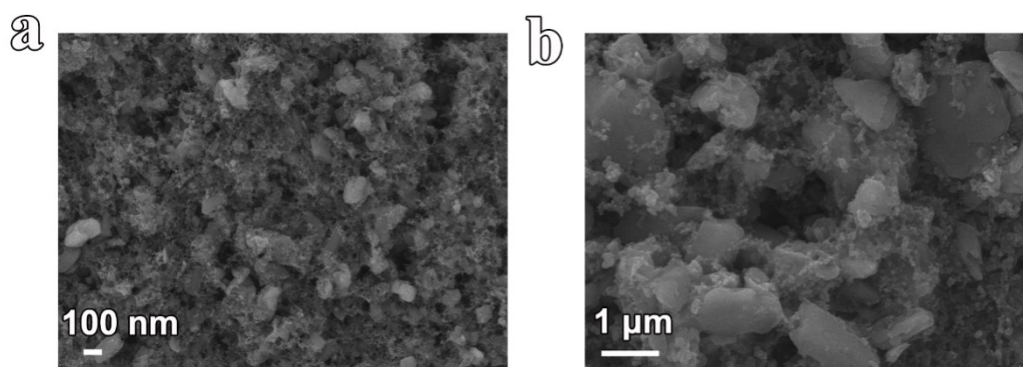


**Fig. S10.** SEM images of S- and L-NiFe MOF after 100 hrs durability test at current density of  $10 \text{ mA cm}^{-2}$  for OER in 1 M KOH electrolyte, which displays negligible change after test and then further demonstrates the strong stability of these NiFe MOFs.

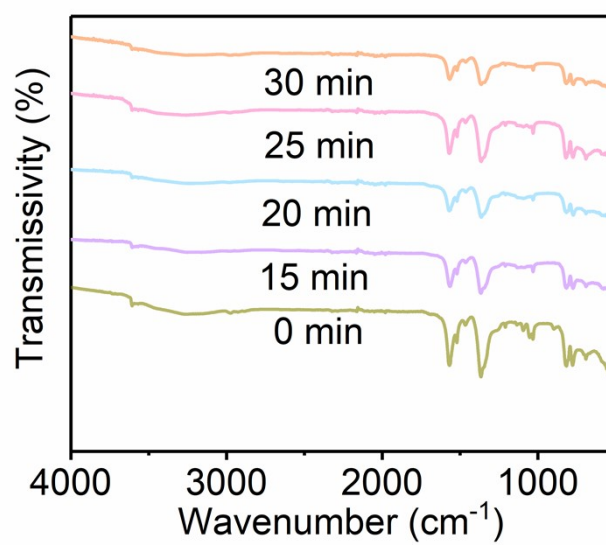


**Fig. S11.** FT-IR spectra of MOFs prepared with other organic ligands (2,5-thiophene dicarboxylic acid).

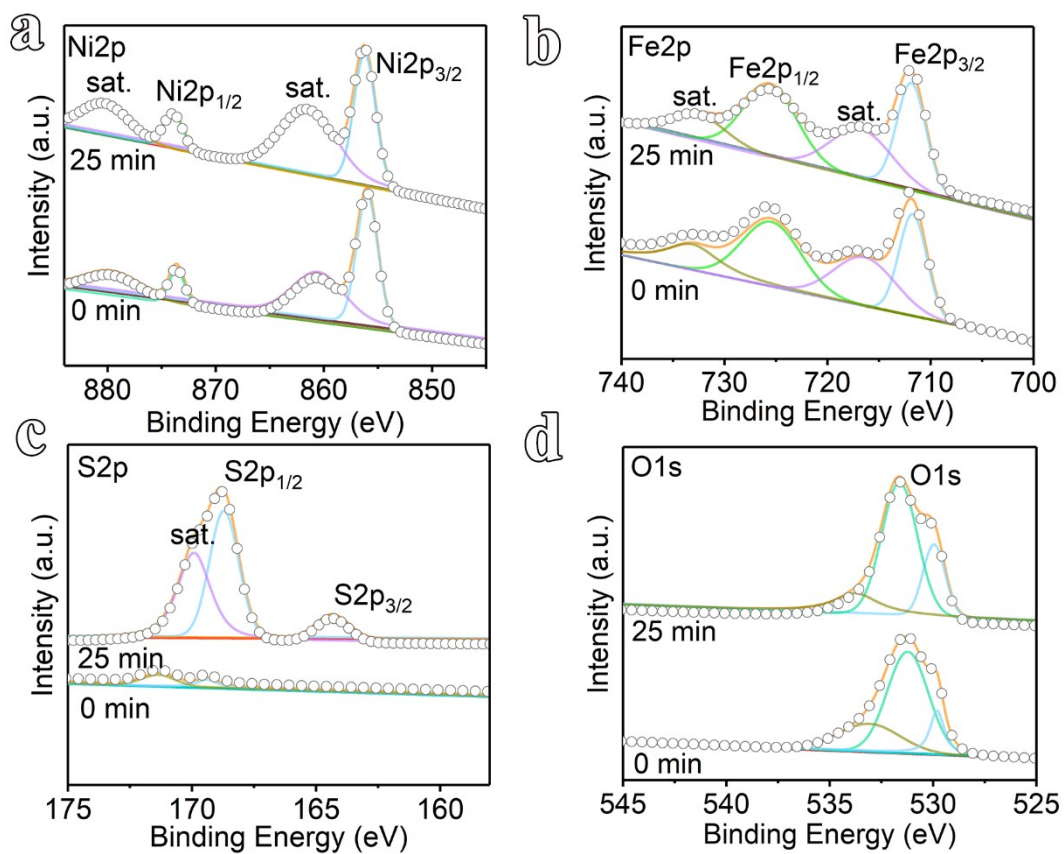


**Fig. S12.** The X-ray photoelectron spectroscopy (XPS) of MOFs prepared with other organic ligands (2,5-thiophene dicarboxylic acid) treated by O<sub>2</sub> plasma for 0 and 25 mins. a) Ni 2p; b) Fe 2p; c) S 2p; d) O 1s. The phenomenon is similar to those of NiFe-MOF particles.

**Table S1.** Theoretical Bader charge transfer data of NiFe-MOFs.

<b>Samples</b>	<b>atoms</b>	<b>Charge transfer</b>
<b>NiFe-MOFs</b>	C <sub>17</sub>	-0.02
	H <sub>20</sub>	0.12
<b>NiFe-MOFs-hydroxyl</b>	C <sub>17</sub>	0.57
	O <sub>13</sub>	-1.12
	H <sub>20</sub>	0.64

**Table S2.** XPS element content of NiFe-MOF particles treated by O<sub>2</sub> plasma for 0 and 20 mins.

<b>Sample</b>	<b>C (At%)</b>	<b>O(At%)</b>	<b>Ni (At%)</b>	<b>Fe (At%)</b>
<b>0 min</b>	57.66	30.23	6.89	5.22
<b>20 min</b>	30.82	55.01	7.53	6.64

**Table S3.** Comparison of the OER activity of S-NiFe-MOF with some recently published OER electrocatalysts.

Catalyst	Electrolyte	$\eta_{10}$ (mV)	Tafel slope (mV dec <sup>-1</sup> )	Reference no.
S-NiFe-MOF	1 M KOH	258	19	This work
L-NiFe-MOF	1 M KOH	298	69	This work
IrO <sub>2</sub>	1 M KOH	368	104	This work
<b>MOF-derived</b>				
Co <sub>3</sub> O <sub>4</sub> /carbon nanowire arrays	0.1 M KOH	290	70	2
NiCo-MOF	1 M KOH	250	42	3
NiFe-UMNs	1 M KOH	260	30	4
NF-PBA	1 M KOH	258	46	5
CoO <sub>x</sub> -ZIF	1 M KOH	400	70	6
Ni@NC	1 M KOH	280	45	7
Ni <sub>3</sub> S <sub>4</sub>	1 M KOH	307	67	8
Co <sub>9</sub> S <sub>8</sub> @TDC	1 M KOH	330	86	9
Co <sub>3</sub> O <sub>4</sub> /CoFe	1 M KOH	297	61	10
A <sub>2.7</sub> B-MOF-FeCo <sub>1.6</sub>	1 M KOH	288	39	11
Co <sub>x</sub> Fe <sub>1-x</sub> -MOF-74	1 M KOH	280	56	12
h-TMCN	1 M KOH	276	82	13
Co-Mo <sub>2</sub> N	1 M KOH	302	90	14
CoFe 2D MOF	1 M KOH	274	46.7	15
Zn <sub>0.1</sub> Co <sub>0.9</sub> Se <sub>2</sub>	1 M KOH	340	43.2	16

---

<b>Co<sub>3</sub>Fe-MOF</b>	1 M KOH	280	38	17
<b>CoFe-MOF</b>	1 M KOH	265	44	18

**Table S4.** XPS element content of MOFs prepared with other organic ligands (2,5-thiophene dicarboxylic acid) treated by oxygen plasma for 0 and 25 mins.

<b>Sample</b>	<b>S(At%)</b>	<b>C(At%)</b>	<b>O(At%)</b>	<b>Ni(At%)</b>	<b>Fe(At%)</b>
<b>0 min</b>	3.95	34.33	40.41	3.61	17.7
<b>25 min</b>	4.04	28.99	46.81	4.56	15.6

## Supporting Reference

- 1 J. Duan, S. Chen and C. Zhao, *Nat. Commun.*, 2017, **8**, 15341.
- 2 T. Y. Ma, S. Dai, M. Jaroniec and S. Z. Qiao, *J. Am. Chem. Soc.*, 2014, **136**, 13925-13931.
- 3 S. Zhao, Y. Wang, J. Dong, C. T. He, H. Yin, P. An, K. Zhao, X. Zhang, C. Gao, L. Zhang, J. Lv, J. Wang, J. Zhang, A. M. Khattak, N. A. Khan, Z. Wei, J. Zhang, S. Liu, H. Zhao and Z. Tang, *Nat. Energy*, 2016, **28**, 1-10.
- 4 G. Hai, X. Jia, K. Zhang, X. Liu, Z. Wu and G. Wang, *Nano Energy*, 2018, **44**, 345-352.
- 5 X. Su, Y. Wang, J. Zhou, S. Gu, J. Li and S. Zhang, *J. Am. Chem. Soc.*, 2018, **140**, 11286-11292.
- 6 S. Dou, C. L. Dong, Z. Hu, Y. C. Huang, J. L. Chen, L. Tao, D. Yan, D. Chen, S. Shen, S. Chou and S. Wang, *Adv. Funct. Mater.*, 2017, **27**, 1702546.
- 7 Y. Xu, W. Tu, B. Zhang, S. Yin, Y. Huang, M. Kraft and R. Xu, *Adv. Mater.*, 2017, **29**, 1605957.
- 8 K. Wan, J. Luo, C. Zhou, T. Zhang, J. Arbiol, X. Lu, B. W. Mao, X. Zhang and J. Fransaer, *Adv. Funct. Mater.*, 2019, **29**, 1900315.
- 9 J. Y. Zhao, R. Wang, S. Wang, Y. R. Lv, H. Xu and S. Q. Zang, *J. Mater. Chem. A*, 2019, **7**, 7389-7395.
- 10 X. Wang, L. Yu, B. Y. Guan, S. Song and X. W. D. Lou, *Adv. Mater.*, 2018, **30**, e1801211.

- 11 Z. Xue, Y. Li, Y. Zhang, W. Geng, B. Jia, J. Tang, S. Bao, H. P. Wang, Y. Fan, Z. W. Wei, Z. Zhang, Z. Ke, G. Li and C. Y. Su, *Adv. Energy Mater.*, 2018, **8**, 1801564.
- 12 X. Zhao, B. Pattengale, D. Fan, Z. Zou, Y. Zhao, J. Du, J. Huang and C. Xu, *ACS Energy Lett.*, 2018, **3**, 2520-2526.
- 13 Z. Kou, T. Wang, Q. Gu, M. Xiong, L. Zheng, X. Li, Z. Pan, H. Chen, F. Verpoort, A. K. Cheetham, S. Mu and J. Wang, *Adv. Energy Mater.*, 2019, **9**, 1803768.
- 14 X. Shi, A. Wu, H. Yan, L. Zhang, C. Tian, L. Wang and H. Fu, *J. Mater. Chem. A*, 2018, **6**, 20100-20109.
- 15 M. Cai, Q. Liu, Z. Xue, Y. Li, Y. Fan, A. Huang, M. R. Li, M. Croft, T. A. Tyson, Z. Ke and G. Li, *J. Mater. Chem. A*, 2020, **8**, 190-195.
- 16 X. Wang, F. Li, W. Li, W. Gao, Y. Tang and R. Li, *J. Mater. Chem. A*, 2017, **5**, 17982-17989.
- 17 W. Li, W. Fang, C. Wu, K. N. Dinh, H. Ren, L. Zhao, C. Liu and Q. Yan, *J. Mater. Chem. A*, 2020, **8**, 3658-3666.
- 18 Z. Zou, T. Wang, X. Zhao, W. J. Jiang, H. Pan, D. Gao and C. Xu, *ACS Catal.*, 2019, **9**, 7356-7364.